Research Square

Preprints are preliminary reports that have not undergone peer review.
They should not be considered conclusive, used to inform clinical practice,
or referenced by the media as validated information.

Hydrothermally synthesised n-n heterostructured ZnO-SnO 2 composites: A novel solution for formaldehyde detection

Naresh Kumar M
CMR Technical Campus
Nagaraju Pothukanuri
nagarajuphysics@gmail.com

Sreenidhi University

Research Article

Keywords: Formaldehyde, ZnO, SnO2, heterostructures, XRD, response.

Posted Date: November 12th, 2026

DOI: https://doi.org/10.21203/rs.3.rs-11509202/v1

License: This work is licensed under a Creative Commons Attribution 4.0 International License.
Read Full License

Additional Declarations: No competing interests reported.

Hydrothermally synthesised n-n heterostructured ZnO-SnO_2 composites: A novel solution for formaldehyde detection

M. Naresh Kumar[1,2], Nagaraju Pothukanuri[3*]

[1]Department of Physics, CMR Technical Campus, Kandlakoya, Medchal, Hyderabad, Telangana State, India.

[2]Bharatiya Engineering Science & Technology Innovation University Gownibaripalli, Anantapur, Andhra Pradesh, India.

[3]Department of Physics, Sreenidhi University, Ghatkesar, Hyderabad, Telangana State, India.

[*]Corresponding author: nagarajuphysics@gmail.com

***

Abstract

This work presents the hydrothermally synthesised and detailed investigation on pure ZnO, SnO_2 and n-n heterostructured ZnO-SnO_2 composite materials for the detection of formaldehyde under ambient conditions. The sensor material was structurally and morphologically characterized by X-ray diffraction technique, Raman spectroscopy, transmission electron microscopy (TEM) and scanning electron microscopy (SEM). Chemical properties of the prepared materials were studied using energy-dispersive X-ray spectroscopy and X-ray photo electron spectroscopy. Gas sensing studies were performed with liquid distribution technique towards various volatile organic compounds such as acetone, benzene, ethanol, methanol and formaldehyde under ambient conditions. Among these gases formaldehyde has shown good response towards n-n heterostructured ZnO-SnO_2 composite material with a response and recovery times of 36s and 24 s under ambient conditions.

Key words

Formaldehyde, ZnO, SnO_2, heterostructures, XRD, response.

1.0.Introduction

Formaldehyde (HCHO) is widely regarded as one of the most toxic volatile organic compounds (VOCs) produced from numerous industrial wastages, building materials, wood furniture, adhesives, paints, textiles, plastics, pharmaceutical products, and household cleaning agents [1]. Continuous exposure to formaldehyde, under low level concentrations, may result in severe

irritation of the eyes, skin and respiratory tract, while prolonged exposure has been associated with asthma, neurological disorders and various forms of cancer [2-3]. Due to these adverse health effects, HCHO has been categorised as a human carcinogen, making its rapid and reliable tracing is important for safeguarding human health, ensuring workplace safety and maintaining indoor air quality. Consequently, the fabrication of extremely sensitive, selective, stable and cost-effective gas sensors capable of detecting low concentrations of formaldehyde has become an important research topic in industrial process control, environmental monitoring, and healthcare diagnostics [4 -5].

Among the various analytical techniques available for HCHO sensing applications, including gas chromatography, mass spectrometry, infrared spectroscopy and optical sensing methods, semiconductor metal oxide (MOS) based chemiresistive gas sensors have captured tremendous recognition because of their simple device architecture, low fabrication cost, rapid response, compact size, less power utilisation and ease of integration into portable electronic devices [6 -7]. The working principle of these gas sensors is based on the change in electrical resistance resulting from surface adsorption and subsequent redox reactions between oxygen ions adsorbed on the semiconductor surface and target gas molecules. The operational efficiency of MOS sensors is therefore governed by various essential components, including the surface chemistry, crystal structure, particle size, morphology, defect concentration, exposed crystal facets, and electronic properties of the sensing material. Consequently, extensive efforts have been devoted to engineering nanostructured metal oxides with improved surface activity and charge transport characteristics to achieve enhanced gas sensing performance [8].

The operational characteristics of metal oxide semiconductor sensors are strongly governed by their structural dimensions and surface characteristics. Nanostructured metal oxides possess a substantially higher specific surface area than bulk materials, allowing a greater density of chemically active sites to participate in gas adsorption. The reduced dimensions also decrease the transport distance for charge carriers, enabling rapid changes in electrical conductivity following surface reactions. As a result, nanostructured sensing materials generally demonstrate enhanced sensitivity and faster response-recovery behaviour [9]. In addition to particle size, the morphology of the sensing material plays a critical role in determining gas diffusion and reaction kinetics. One-dimensional (nanowires and nanorods), two-dimensional (nanosheets), and three-dimensional (hollow, porous, and hierarchical) architectures provide different pathways for gas transport and electron conduction. Optimizing these structural features improves the accessibility of reactive sites, facilitates efficient gas diffusion, and

ultimately enhances the overall sensing characteristics of chemiresistive metal oxide sensors [10].

Among different semiconductor oxides, zinc oxide (ZnO) has gained as the most extensively reported gas sensing materials owing to its large direct band gap (~3.37 eV), wide exciton binding energy, remarkable chemical stability, low toxicity, high electron mobility and ease of synthesis into diverse nanostructured materials. ZnO shows remarkable sensitivity towards numerous reducing and oxidizing gases due to its high surface properties and efficient adsorption of oxygen species [11-12]. Moreover, its compatibility with different synthesis methods enables fine-tuned control of particle size, surface morphology and crystallinity. Nevertheless, pristine ZnO sensors often suffer challenges including relatively high operating temperatures, low selectivity and moderate sensing response, restricting their practical applications for selective formaldehyde sensing. Tin dioxide (SnO_2) is another widely researched n-type semiconductor material with an extended bandgap of ~3.6 eV, high electron mobility, good thermal stability and excellent chemical durability. SnO_2-based gas sensors generally show relatively high response toward volatile organic compounds due to of their strong interaction with chemisorbed oxygen species [13]. However, similar to ZnO, pure SnO_2 frequently experiences drawbacks such as slow recovery, poor selectivity and limited long-term stability under varying environmental conditions. These limitations have attracted researchers' attention to design composite and heterostructured sensing materials that combine the complementary advantages of various metal oxides.

Constructing ZnO-SnO_2 heterostructures has evidenced to be an alternative strategy for significantly improve gas sensing studies. Since both ZnO and SnO_2 are popular semiconductors with electrons as majority carriers possessing various work functions and band alignment structures, intimate contact between them results in the formation of an n-n heterojunction [14]. Upon contact, electrons migrate from one semiconductor to the other until equilibrium of the Fermi levels is attained, producing expanded depletion regions and interfacial potential barriers. These interfacial electronic changes considerably affect charge transport mechanism during gas adsorption and desorption processes during gas sensing mechanism. Exposure to reducing gases such as formaldehyde changes the width of depletion layer and barrier height more effectively than in single-component oxides, thereby generating higher resistance variations and improved sensor response [15]. Apart from electronic sensitization, the synergistic effect between ZnO and SnO_2 enhances oxygen adsorption capacity, promotes catalytic surface reactions and facilitates efficient electron transfer across

the heterointerface, collectively contributing to superior sensing studies. Beyond heterojunction engineering, controlling the morphology of ZnO-SnO_2 composites further enhances sensing behaviour. Nanostructured composite materials possessing porous frameworks, interconnected nanoparticles, hierarchical architectures or one-dimensional nanostructures provide abundant active sites and facilitate rapid diffusion of gas molecules throughout the sensing layer [16-17]. The improved surface area promotes higher oxygen adsorption, while the interconnected porous pathways accelerate adsorption-desorption kinetics, showing in faster response and recovery properties. Furthermore, decreasing crystallite size to values comparable with the Debye length allows the entire particle volume to participate in the gas sensing process, leading to wider optimization of electrical conductivity upon exposure to target gases during the gas sensing measurements [18].

Among the available synthesis approaches, the hydrothermal technique has become one of the most attractive methods for synthesising ZnO-SnO_2 nanocomposite materials because of its simplicity, low processing temperature, scalability and excellent control over crystal growth. In hydrothermal synthesis process, chemical kinetics take place in a sealed aqueous environment under elevated temperature and pressure, creating homogeneous nucleation and controlled crystal development [19]. Compared with conventional solid-state or high-temperature techniques, hydrothermal processing offers several advantages, including high crystallinity, small particle size distribution, enhanced phase purity, controllable surface morphology and reduced agglomeration. By carefully adjusting reaction variables like solution pH, reaction temperature, concentration of precursor, duration and surfactant concentration, various ZnO-SnO_2 architectures including nanoparticles, nanorods, nanowires, nanosheets, hollow structures and hierarchical composites can be synthesized reproducibly. These advantages make the hydrothermal method particularly suitable for developing high-performance gas sensing materials with tailored structural and surface properties.

Hydrothermally synthesized ZnO-SnO_2 n-n heterostructured composites have demonstrated remarkable gas sensing performances toward various hazardous gases, such as NO_2, methanol, acetone, CO, ethanol, and other toxic volatile organic compounds. Earlier studies have consistently reported that these composites show higher response, enhanced selectivity, faster response-recovery kinetics and lower working temperatures than pure ZnO or SnO_2 due to the combined effects of n-n heterojunction formation, enhanced oxygen adsorption and optimized nanostructured morphology. These findings exhibit that rational design of ZnO-SnO_2

heterostructures demonstrates an effective route for developing next-generation semiconductor gas sensors capable of detecting hazardous VOCs with improved analytical performance.

Despite substantial development in ZnO-SnO_2-based gas sensing materials, reports focusing specifically on hydrothermally synthesized ZnO-SnO_2 composites for formaldehyde detection remain relatively limited. Since formaldehyde possesses unique adsorption and oxidation characteristics compared with other reducing gases, further investigation is necessary to optimize the structural, morphological and interfacial properties of ZnO-SnO_2 composites for selective and sensitive HCHO detection [20-21]. Henceforth, the current research aims to synthesize ZnO-SnO_2 composite nanoparticles through a facile hydrothermal route and systematically investigate their structural, morphological, optical and gas sensing properties towards formaldehyde. The relationship between heterojunction formation, microstructural evolution and sensing behaviour is discussed to establish the role of ZnO-SnO_2 nanocomposites in enhancing formaldehyde sensing performance and to provide useful insights for the design of efficient VOC sensing materials.

2.0 Synthesis of ZnO, SnO_2 and ZnO-SnO_2 nanocomposites

Pure ZnO and SnO_2 nanoparticles were synthesized separately via a hydrothermal route using analytical-grade precursors in their original supplied form. Zinc acetate dihydrate ($Zn(CH_3COO)_2 \cdot 2H_2O$, 99.9%, Sigma-Aldrich, India) and tin (IV) chloride pentahydrate ($SnCl_4 \cdot 5H_2O$, 99.9%, Sigma-Aldrich, India) were employed as the zinc and tin sources, respectively. Deionized (DI) water (Thermo Fisher Scientific, India) was used as the solvent throughout the synthesis. For the preparation of ZnO nanoparticles, an appropriate amount of zinc acetate dihydrate was incorporated in DI water under continuous magnetic stirring until a homogeneous solvent was obtained. Thereafter, sodium hydroxide (NaOH) solution was added dropwise while stirring process to adjust the pH of the solution to approximately 10. The obtained clear solution was blended for subsequent 30 min to achieve a unform precursor solution and then poured to a 50 mL Teflon-lined stainless-steel autoclave. The autoclave was air tightly closed and preserved at 180 °C in a hot air oven for about 16 h to facilitate hydrothermal crystallization. Then after naturally cooling to room temperature, the resulting precipitate was collected by filtration using Whatman filter paper, thoroughly rinsed multiple times with deionized water to eliminate residual ion species and impurities, and dried. Finally, the obtained powder was calcined in a muffle furnace at 300 °C for 3 h to improve its crystallinity. SnO_2 nanoparticles were synthesized following the same hydrothermal procedure.

Tin (IV) chloride pentahydrate was dissolved in DI water and magnetically stirred up to a clear solution was generated. The solution pH was maintained at around 10 by the gradual incorporation of sodium hydroxide precursor under prolonged stirring. The precursor solution was then transferred into a Teflon-lined stainless-steel autoclave and hydrothermally treated at 180 °C for 16 h. After cooling, the precipitate was filtered, repeatedly washed with deionized water, dried, and subsequently calcined at 300 °C for 3 h. The ZnO-SnO_2 nanocomposite containing 50 wt.% ZnO and 50 wt.% SnO_2 was synthesized by mixing the estimated quantity of zinc acetate dihydrate and tin (IV) chloride pentahydrate in deionized water to achieve the desired weight ratio. The mixed precursor solution was magnetically stirred until homogeneous, after which sodium hydroxide solution was mixed dropwise to adjust the pH to approximately 10. The uniform suspension was added into a Teflon-lined stainless-steel autoclave for hydrothermal procedure at 180 °C for 16 h. The obtained product was filtered using Whatman filter paper, multiple washing cycles with DI water to eliminate residual precursor species, dried, and finally calcined in a muffle furnace at 300 °C for 3 h. The hydrothermal process promoted the simultaneous crystallization of ZnO and SnO_2 nanoparticles, resulting in the formation of an intimately contacted ZnO-SnO_2 heterostructured nanocomposite suitable for gas sensing applications.

2.1. Characterization techniques

The crystal structure and phase composition of the synthesized ZnO, SnO_2, and ZnO–SnO_2 nanomaterials were examined using X-ray diffraction (XRD) (Rigaku Ultima IV Powder X-ray Diffractometer, Rigaku, Japan) employing Cu Kα source ($\lambda = 1.5406$ Å). X-ray diffraction data were acquired over a 2θ range of 20°- 80° with the instrument working at an accelerating potential of 60 kV. The surface morphology and microstructure of the prepared samples were investigated with a SEM (Hitachi SU3800, Hitachi, Japan). The detailed nanostructure, particle size, crystallinity, and lattice fringes of the synthesized nanoparticles were further characterized using TEM (Tecnai G2 Spirit BioTWIN, FEI, Netherlands). Raman spectroscopy is used to identify and investigate the vibrational properties, chemical bonding, and structural characteristics of prepared samples.

The chemical composition and ionic states of the constituent species, and electronic interactions within the nanocomposites were investigated by X-ray photoelectron spectroscopy (XPS) using a Kratos/Shimadzu ESCA-3400 spectrometer.

2.2. Fabrication sensor element for gas sensor applications

The hydrothermally synthesized powders were dispersed in acetone to form a uniform paste. The prepared paste was homogeneously coated onto thoroughly cleaned glass substrates using the doctor blade method to obtain a sensing film of uniform thickness. The coated films were subsequently dried and annealed at 150 °C to improve solvent evaporation, film adhesion, and mechanical stability. After annealing, two parallel electrodes were fabricated on the sensing film using commercially available silver paste. The electrode-patterned sensors were further heated at 150 °C for 30 min to ensure good electrical connections and strong adhesion between the sensing element layer and the printed electrodes. The fabricated sensor element was mounted inside a custom-designed stainless-steel gas sensing measurement compartment made with electrical feedthroughs for resistance measurements. Desired concentrations of formaldehyde vapour were generated by injecting a calculated volume of liquid formaldehyde into the sealed chamber using a calibrated microsyringe. The vapour concentration was estimated using the following empirical equation [22].

$$\text{Concentration of analyte gas (C ppm)} = \frac{22.4 \times V1 \times \rho \times \text{ø}}{V2 \times M} \quad \text{……..(1)}$$

In the above equation, V_1 is volume of the analyte solution, ρ is the density of liquid to be poured into the gas sensing measurement chamber, ø is the fraction of liquid evaporated, V_2 is the volume of testing compartment, M is the molecular weight (molar mass) of the target gas.

The electrical resistance of the sensing element was continuously monitored under both dry air and target gas atmospheres at a relative humidity of 60% with a Keithley 6517B electrometer interfaced with a computer for real-time data acquisition. The sensor response was determined from the change in electrical resistance upon exposure to formaldehyde vapour. Each sensing measurement was repeated several times to ensure the reproducibility and reliability of the obtained results.

$$\text{Response (R)} = \frac{R_a}{R_g} \quad \text{…….(2)}$$

3.0 Results and Discussion

3.1. X-Ray diffraction

The phase composition and crystallographic characteristics of the hydrothermally synthesized ZnO, SnO_2 and 50 wt.% ZnO-50 wt.% SnO_2 nanocomposites were investigated using X-ray diffraction (XRD), as shown in Fig. 1. The diffraction peaks of pure ZnO are indexed to the hexagonal wurtzite phase (space group $P6_3mc$), with the characteristic reflections related to the (100), (002), (101), (102), (110), (103), (200), (112), (201), (004), and (202) planes, which are

well agreement with the JCPDS Card No. 36-1451 [23]. Among these reflections, the (101) crystal plane shows the highest diffraction intensity, showing its preferential orientation and excellent crystallinity. The nonexistence of other diffraction peaks validates the phase purity of the prepared ZnO nanoparticles. Whereas, the X-ray diffraction pattern of SnO_2 displays diffraction peaks indexed to the tetragonal rutile phase (space group $P4_2/mnm$), related to the (110), (101), (200), (211), (220), (310), (112), (202), and (321) crystallographic indices, which are in excellent agreement with JCPDS Card No. 41-1445 [24]. No impurity peaks related to SnO or other tin oxide phases are identified, demonstrating the successful formation of single-phase high pure crystalline SnO_2. The diffraction pattern of the ZnO-SnO_2 nanocomposite simultaneously exhibits the characteristic reflections of both ZnO and SnO_2, demonstrating the coexistence of the two crystalline phases without any other detectable secondary compounds [25-26]. The absence of shifting of peaks or additional diffraction reflections recommends that the composite consists of a physical heterojunction rather than substitutional solid-solution formation, owing to the considerable difference in crystal structures and lattice parameters between ZnO and SnO_2 [27]. And also, the diffraction peaks of the composite become noticeably wider with decreased intensity compared to those of the pure oxides. Such peak broadening indicates the formation of smaller crystallites and increased lattice imperfections generated during heterogeneous nucleation and formation of the composite [28]. The average crystallite size determined with the Scherrer formula decreases from 9.60 nm for ZnO and 7.30 nm for SnO_2 to 5.97 nm for the ZnO-SnO_2 nanocomposite. This significant decrement reflects that the interfacial interaction between ZnO and SnO_2 effectively suppresses crystal growth at the time of hydrothermal synthesis. The formation of ultrafine crystallites enhances the specific surface area, exposes a larger number of active adsorption sites, and enhances the density of grain boundaries and n-n heterojunction interfaces.

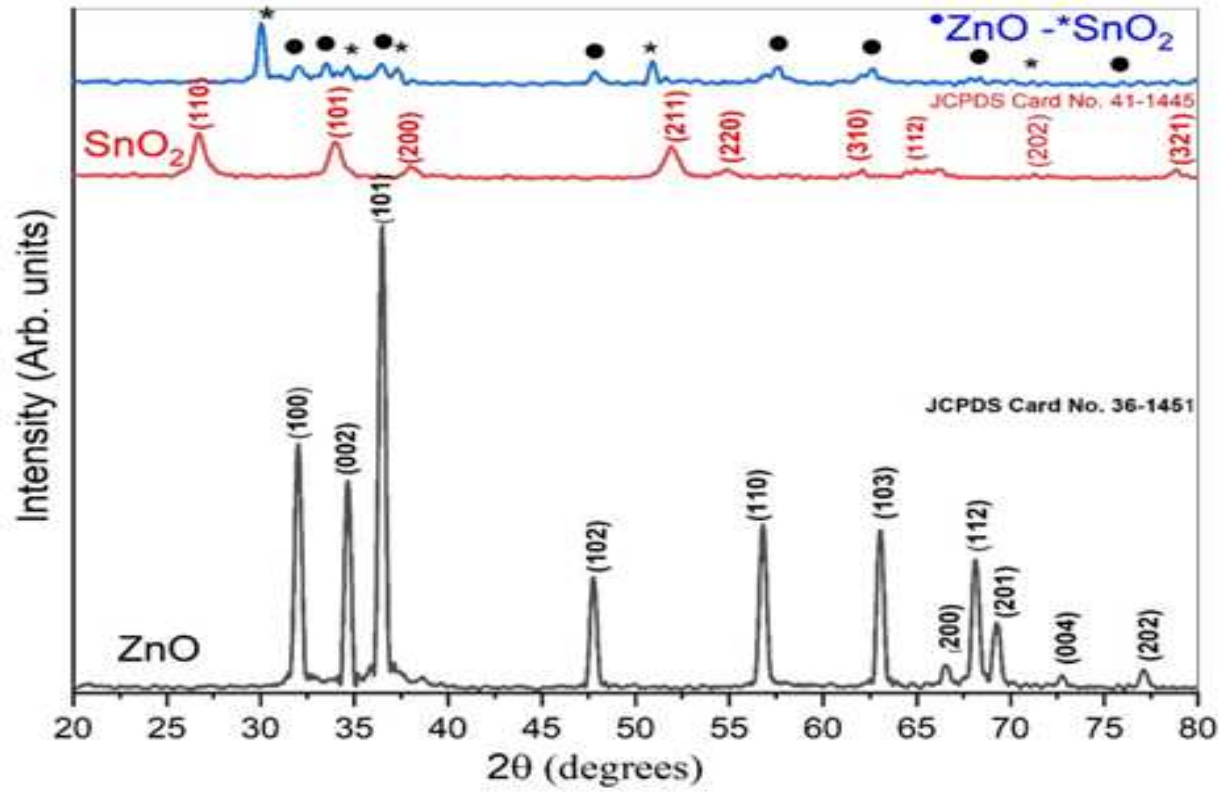


Fig.1. XRD patterns of ZnO, SnO_2 and ZnO-SnO_2 composites

These structural properties are highly advantageous for chemiresistive gas sensing because they promote oxygen adsorption, enlarge the electron depletion region, and facilitate more efficient modulation of charge transport upon exposure to formaldehyde molecules. Consequently, the reduced crystallite size together with the formation of abundant ZnO-SnO_2 heterointerfaces is expected to substantially enhance the sensitivity, response kinetics, and detection capability of the nanocomposite sensor compared with the individual oxide counterparts.

Crystallite size, dislocation density and micro-strain were estimated using the below relations [29].

$$\text{Crystallite size (D)} = \frac{K\,\lambda}{\beta\,Cos\,\theta} \quad \text{.....(1)}$$

$$\text{Dislocation density } (\delta) = \frac{1}{(\text{Crystallite size})^2} \quad \text{.....(2)}$$

$$\text{Micro strain } (\varepsilon) = \frac{\beta Cos\theta}{4} \quad \text{.....(3)}$$

Table 1. Structural parameters of ZnO, SnO_2 and ZnO-SnO_2 composites

S. No	Sample	Crystallite size (nm)	Dislocation density $\times 10^{16}$ (lines/m^2)	Strain $\times 10^{-3}$
1	Pure ZnO	9.6	1.09	2.20
2	Pure SnO_2	7.3	1.88	2.87
3	ZnO-SnO_2 composite	5.97	2.81	4.55

3.2. Morphological studies

The FESEM micrographs of the hydrothermally synthesized samples reveal significant changes in morphology with the formation of the ZnO-SnO_2 nanocomposite. As depicted in Fig. 2(A), pure ZnO consists mainly of uniformly scattered hexagonal rod-like and short prismatic crystallites with well-defined facets, reflecting the anisotropic crystal growth characteristic of the hexagonal wurtzite structure [30]. Whereas a slight agglomeration is observed, numerous interparticle voids are retained, exhibiting an interconnected porous network that facilitates gas diffusion. In contrast, the pure SnO_2 sample as shown in Fig. 2(B) displays irregularly shaped spherical and cauliflower-like nanoparticle aggregates formed by the agglomeration of ultrafine primary nanoparticles [31]. These closely packed clusters possess a relatively rough surface texture with abundant grain boundaries but comparatively fewer open diffusion channels than pure ZnO. Interestingly, the 50 wt.% ZnO-50 wt.% SnO_2 nanocomposite as represented in Fig.2 (C) combines the morphological features of both constituents, where rod-like ZnO crystallites are uniformly embedded within a matrix of fine SnO_2 nanoparticles. The intimate interfacial contact between the two oxides results in a hierarchical porous architecture comprising coarse crystallites decorated with nanosized particles. This heterogeneous morphology substantially enhances the density of active adsorption sites, interparticle n-n junctions, and exposed grain boundaries while maintaining sufficient open porosity for efficient gas transport. The coexistence of larger crystalline domains and ultrafine nanoparticles is expected to promote rapid adsorption-desorption kinetics and facilitate effective charge transfer across the ZnO-SnO_2 heterojunctions. Consequently, the composite surface morphology enables a larger accessible surface area and improved diffusion pathways compared with the individual oxides, making it highly favourable

for increased gas sensing properties at room temperature through enhanced surface reactivity and efficient modulation of the electrical resistance.

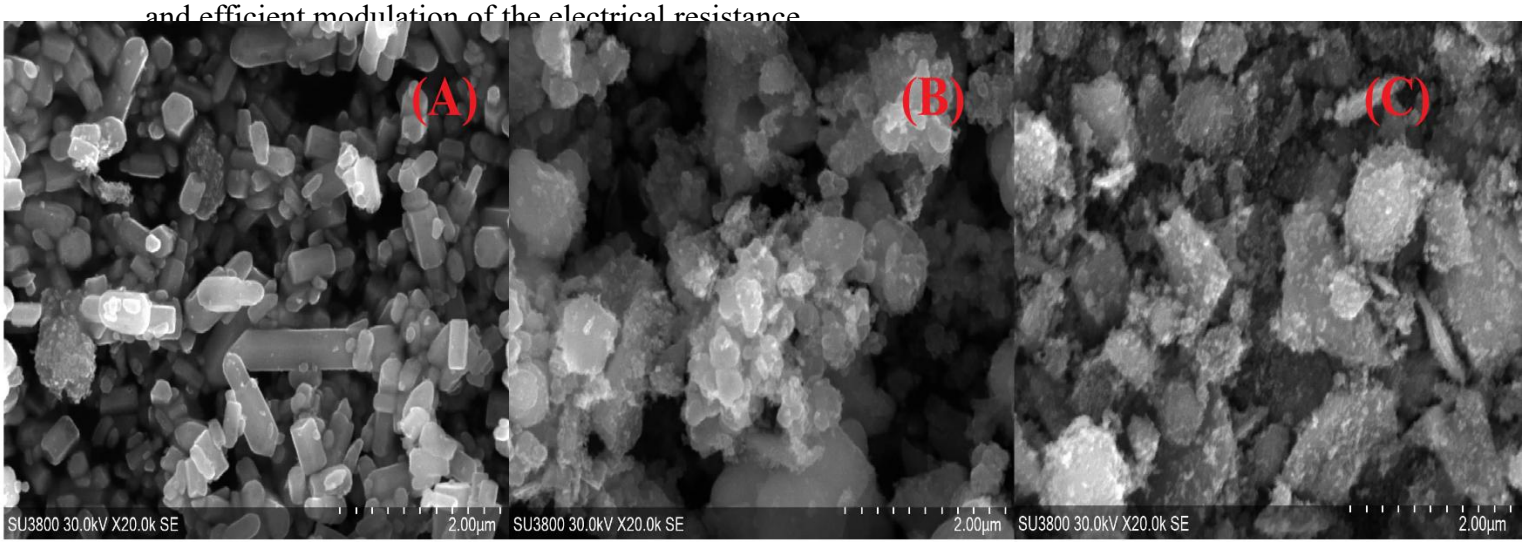


Fig.2. SEM images of (A) ZnO (B) SnO_2 (C) ZnO-SnO_2 composites

3.3. EDX studies

The energy-dispersive X-ray spectroscopy (EDX) spectra depicted in Fig. (A–C) confirm the elemental composition of the hydrothermally synthesized ZnO, SnO_2, and ZnO-SnO_2 nanocomposite, respectively. EDX analysis is a widely used method for identifying the constituent chemical elements of nanostructured materials through the characteristic X-rays emitted during electron-beam irradiation. The observed peak positions are consistent with the characteristic X-ray transition energies of the corresponding elements [32]. In Fig. 3(A), the EDX spectrum of ZnO exhibits an important peaks related to oxygen (O) and zinc (Zn). The oxygen K-line appears at approximately 0.52 keV, while the intense Zn L-line is observed near 1.0 keV. The additional Zn K-line peaks at approximately 8.6 and 9.6 keV further confirm the presence of zinc [33]. The strong Zn signal reflects that zinc is a major constituent of the analysed region, while the oxygen peak supports the formation of zinc oxide. The relative peak intensities are affected by the elemental concentration, excitation conditions, and instrumental response. Fig. 3(B) shows the EDX spectrum of SnO_2, in which the oxygen K-line and characteristic tin (Sn) peaks are observed. The prominent Sn L-line appears around 3.4-3.9 keV, accompanied by lower-energy Sn M-line features. These characteristic reflections confirm the presence of tin and oxygen, consistent with the expected composition of tin dioxide. In Fig. 3(C), the ZnO-SnO_2 composite exhibits characteristic peaks of Zn, Sn, and O simultaneously. The Zn L- and K-lines, Sn L- and M-lines, and oxygen K-line collectively show the coexistence of the constituent elements in the composite. Similar elemental signatures have been reported in EDX investigations of ZnO-SnO_2 nanocomposites.

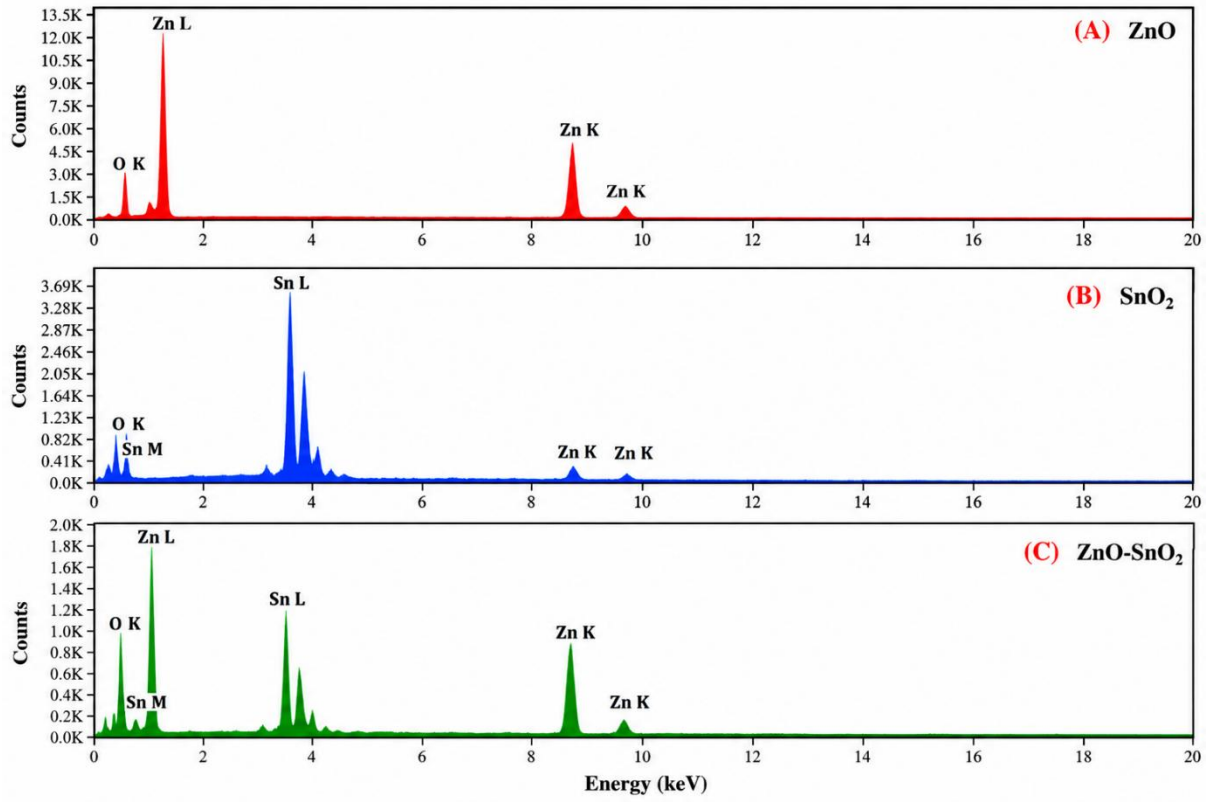


Fig.3. EDX spectra of (A) ZnO (B) SnO_2 (C) ZnO-SnO_2 composites

3.3. Raman studies

Raman spectroscopy was used to investigate the vibrational characteristics and structural features of hydrothermally synthesized ZnO, SnO_2, and ZnO-SnO_2 nanocomposites. Fig. 4 presents the Raman spectra of hydrothermally synthesized (a) ZnO nanoparticles, (b) SnO_2 nanoparticles, and (c) the ZnO-SnO_2 composite. Raman spectroscopy provides information about lattice vibrations and crystal structures, enabling the identification of characteristic vibrational modes associated with the constituent metal oxides.

The spectrum of ZnO reveals a prominent band at 437 cm^{-1}, related to the E_2 (high) phonon mode of hexagonal wurtzite ZnO. This mode is widely identified as a characteristic fingerprint of the wurtzite structure. Additional features near 99 and 330 cm^{-1} are commonly associated with the E_2 (low) mode and a second-order Raman process, respectively. A feature near 574 cm^{-1} may be assigned to the A1 (LO) mode [34]. Whereas, the SnO_2 spectrum displays characteristic Raman bands near 475, 633, and 775 cm^{-1}, assigned to the E_g, A_{1g}, and B_{2g} modes, respectively. These vibrational modes are characteristic of tetragonal rutile SnO_2. The relatively intense A_{1g} mode is associated with symmetric Sn-O bond vibrations, whereas the and E_g and

B_{2g} modes arise from other characteristic lattice vibrations [35]. The ZnO-SnO_2 composite spectrum exhibits feature in the regions associated with both constituent oxides, including bands near 437 and 475-775 cm^{-1}. Their coexistence is consistent with contributions from ZnO and SnO_2 vibrational modes which are in line according to the XRD investigations.

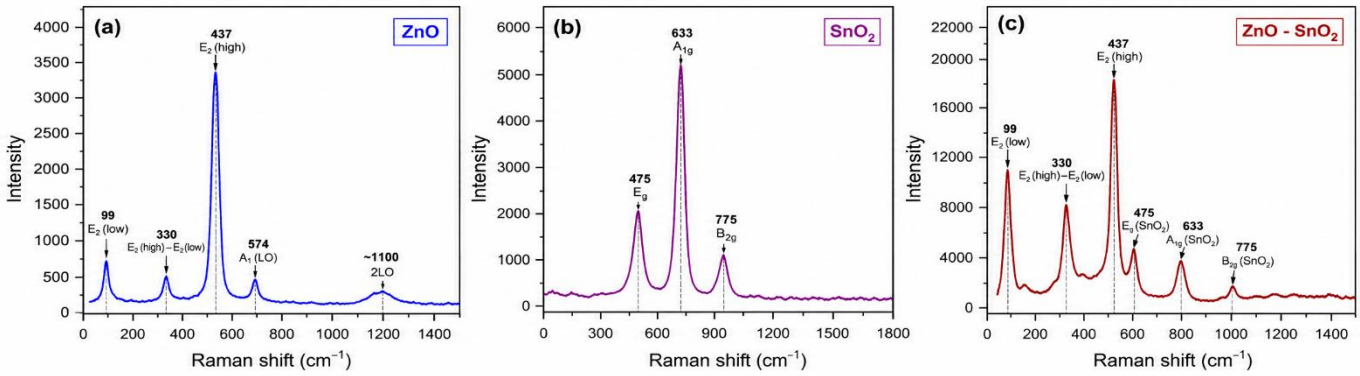


Fig.4. Raman spectra of (a) ZnO, (b) SnO_2, (c) ZnO-SnO_2 composites

3.4. TEM analysis

Fig. 5 (A-C) presents the TEM micrographs of pristine ZnO, SnO_2, and ZnO-SnO_2 nanocomposites, respectively, providing insights into their morphological characteristics, particle distribution, and agglomeration behavior. The TEM micrograph of pristine ZnO as shown in Fig.5(A) reveals the formation of irregularly shaped nanoparticles with predominantly quasi-spherical and faceted morphologies [36]. The particles manifest noticeable changes in size and are extensively agglomerated, resulting in the development of relatively wide clusters [37]. The overlapping particles and variations in image contrast recommend differences particle superposition. Such agglomeration may attain from the high surface energy of nanoparticles and interparticle attractive forces. In contrast, the TEM image of pure SnO_2 as shown in Fig. 5(B) demonstrates the presence of comparatively smaller nanoparticles with predominantly quasi-spherical and slightly irregular morphologies. These nanoparticles are interconnected, generating chain-like and loosely aggregated structures. The relatively distinguishable particle boundaries show the formation of nanoscale particles, although localized agglomeration is evident. The reported morphology suggests the presence of interparticle contact regions that may facilitate charge transport within the sensing material. Interestingly, the TEM micrograph of the ZnO-SnO_2 nanocomposite as shown in Fig. 5(C) provides a heterogeneous morphology consisting of fine nanoparticles distributed around and over larger aggregated structures. The coexistence of differently sized particles and their

intimate physical contact suggest successful morphological integration of the constituent materials. The smaller nanoparticles present to decorate the surfaces of larger agglomerates, potentially enhancing the number of interfacial contact regions. Such interfaces may promote the formation of n-n heterojunctions between ZnO and SnO_2, depending on their electronic band alignment and interfacial charge redistribution [38]. These heterointerfaces can effects charge-carrier transport, surface oxygen adsorption, and subsequent interactions with target gas molecules during the gas sensing measurements. Consequently, the obtained ZnO-SnO_2 composite morphology may be useful for gas-sensing applications by providing additional interfacial regions and potentially accessible reactive sites.

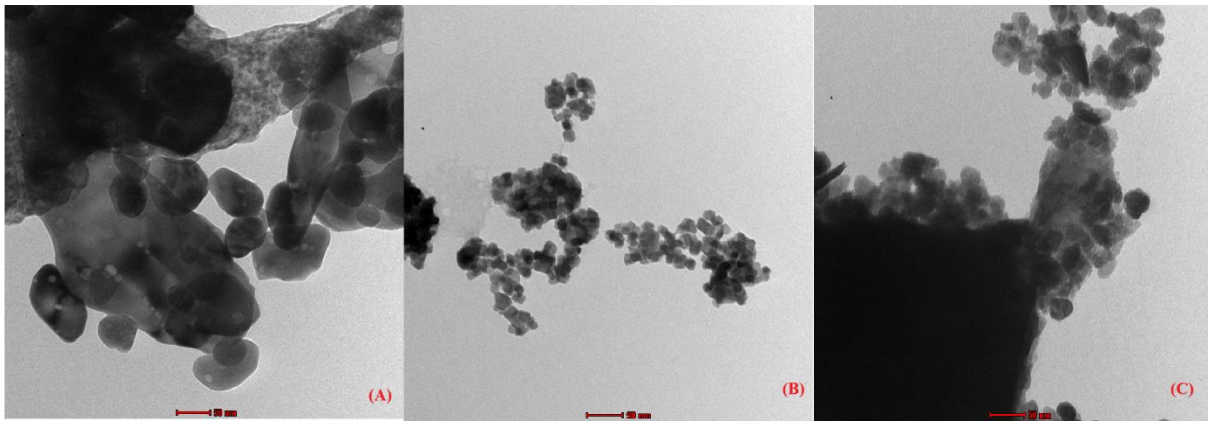


Fig.5. TEM images of (A) ZnO (B) SnO_2 and (C) ZnO-SnO_2 composite

3.5. XPS studies

The X-ray photoelectron spectroscopy (XPS) survey scan spectra of hydrothermally synthesized (A) ZnO, (B) SnO_2, and (C) ZnO-SnO_2 hetero junction nanocomposite are shown in Fig. 6. The survey spectra were obtained to identify the constituent elements oxidation state and evaluate the surface chemical composition of the synthesized materials. As shown in Fig. 6(A), the ZnO sample represents characteristic photoelectron signals related with zinc and oxygen atoms. The prominent Zn 2p doublet, typically appeared near 1022.40 eV and 1045.56 eV, corresponds to Zn $2p_{3/2}$ and Zn $2p_{1/2}$, respectively, confirming the presence of Zn^{2+} in the oxide structure. The O 1s signal, generally located around 531 eV, is associated primarily with lattice oxygen in Zn-O bonds. Additional signals may arise from other zinc core levels and Auger transitions. These observations agree with reported XPS investigations of ZnO-based

nanomaterials. In Fig. 6 (B), the survey spectrum of SnO_2 displays characteristic signals associated with tin and oxygen. The Sn 3d doublet, typically located near 487.36 eV and 495.75 eV, is attributed to Sn $3d_{5/2}$ and Sn $3d_{3/2}$, respectively, supporting the presence of tin in its oxidized state. The O 1s signal further confirms the oxygen-containing oxide structure. These assignments are consistent with published studies of tin oxide and ZnO-SnO_2 heterostructures. As illustrated in Fig. 6(C), the ZnO-SnO_2 composite exhibits characteristic signals attributable to both zinc- and tin-containing species, together with oxygen. The simultaneous appearance of these elemental signals supports the successful incorporation of both oxide components in the composite. Similar XPS survey features have been reported for hydrothermally synthesized ZnO-SnO_2 heterostructures.

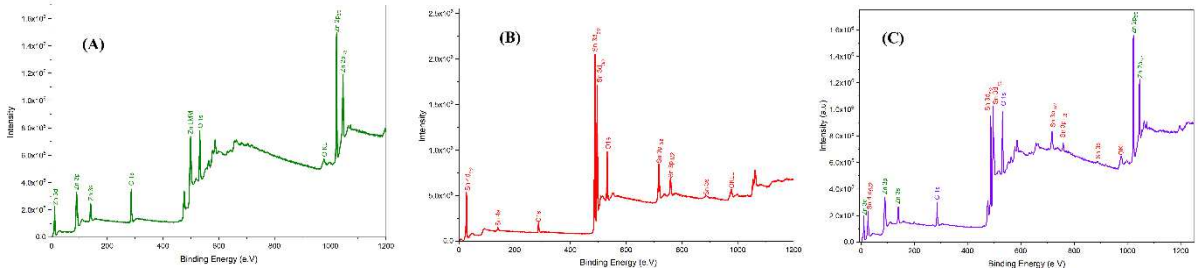


Fig.6. XPS full scan spectra of (A) ZnO (B) SnO_2 (C) ZnO-SnO_2

The deconvoluted X-ray photoelectron spectroscopy (XPS) spectra in Fig. 7(A) exhibit two characteristic peaks related to Zn $2p_{3/2}$ and Zn $2p_{1/2}$, located at approximately 1022.40 and 1045.56 eV, respectively. These peaks confirm the presence of zinc in the ZnO and ZnO-SnO_2 composite samples, with the binding energies being characteristic of Zn^{2+} in ZnO [39]. The spin–orbit splitting of approximately 23.16 eV is consistent with the Zn 2p doublet. Figure (B) displays the Sn 3d core-level spectra, with peaks assigned to Sn $3d_{5/2}$ and Sn $3d_{3/2}$ at approximately 487.36 and 495.75 eV, respectively. The corresponding spin-orbit splitting of approximately 8.39 eV is characteristic of Sn^{4+} in SnO_2 [40]. The observed peaks confirm the coexistence of Zn- and Sn-based oxide species in the composite. Differences in peak intensity and line shape between the pristine oxides and the composite may indicate changes in the local chemical environment following heterostructure formation

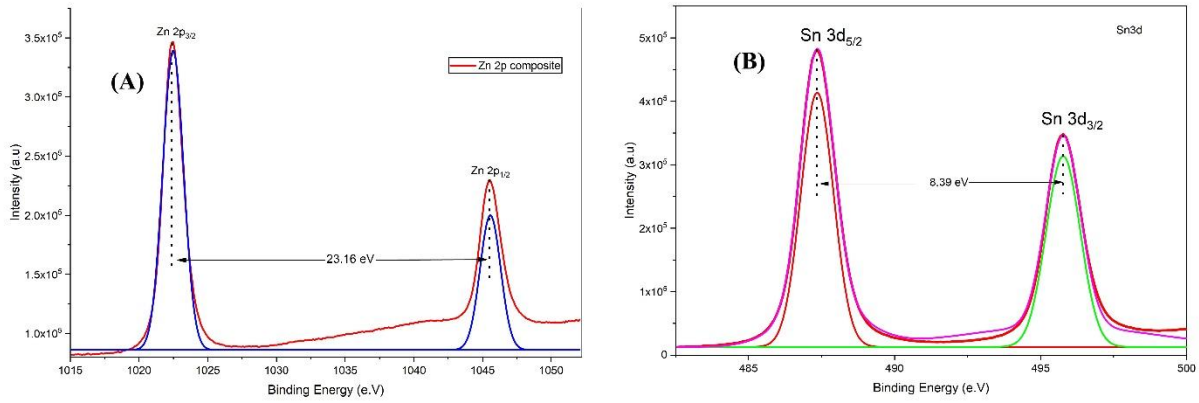


Fig.7. Deconvoluted high-resolution XPS spectra of (A) Zn 2p core-level spectra and (B) Sn 3d core-level

4.Gas sensor applications

4.1. Selectivity

Selectivity is a critical performance parameter of metal oxide semiconductor (MOS) gas sensors, describing their ability to distinguish a target analyte from other interfering gases or present in the surrounding atmosphere. Sensor selectivity is governed by several factors, including the molecular structure and functional groups of the analyte, adsorption affinity, surface reaction kinetics, operating temperature, oxygen vacancy concentration, and the nature of the sensing material. The interaction between the target gas and chemisorbed oxygen species on the metal oxide surface modifies the charge-carrier concentration and, consequently, the electrical resistance of the sensing layer. Differences in molecular adsorption and surface oxidation pathways can therefore produce distinct sensing responses to different gases. Furthermore, heterojunction formation and defect engineering can modify the surface electronic structure and interfacial charge transport, potentially enhancing the discrimination of target gases. Fig.8 shows selectivity of ZnO, SnO_2 and ZnO-SnO_2 towards various target gases such as formaldehyde, acetone, methanol, ethanol and benzene under ambient conditions. From the selectivity study, it is clear that the response towards 5 ppm of formaldehyde is superior in comparing with other target gases. It might be due the bond dissociation energies of the target gases and surface morphologies of the samples [41].

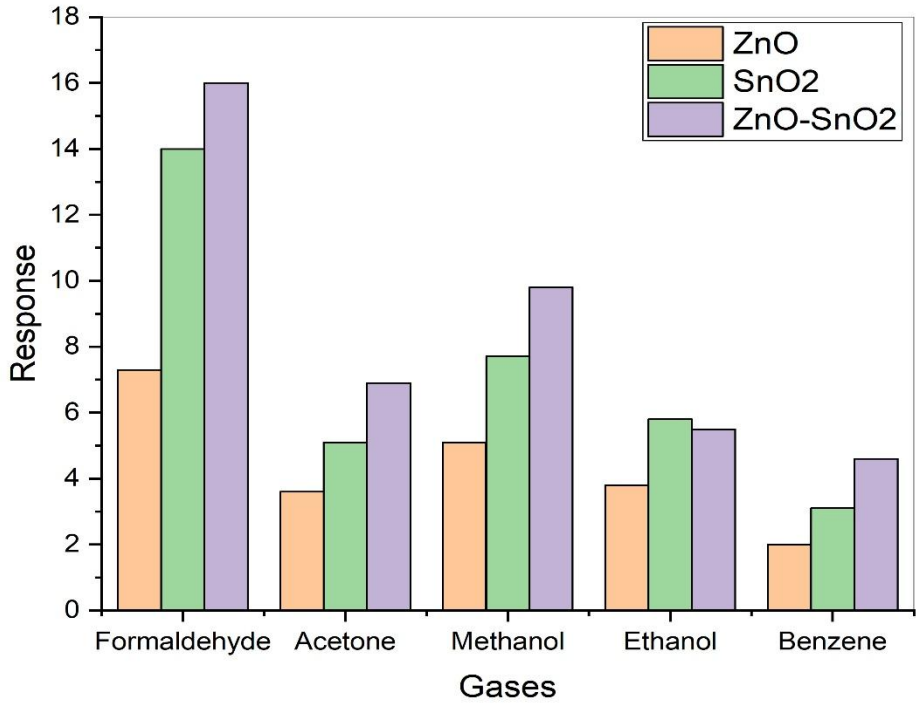


Fig.8. Selectivity response of different gas sensors toward formaldehyde and other interfering volatile organic compounds (VOCs)

4.2. Long term stability

Long term stability is an essential parameter for evaluating the reliability and practical applicability of various gas sensors. It refers to the ability of a sensor to maintain a consistent response toward a target gas over repeated exposure-recovery cycles and extended periods of operation. It is affected by the micro-structural integrity of the sensing material, surface defects, grain growth mechanism, oxygen adsorption-desorption processes, and environmental conditions. Formation of heterostructure (n-n) can potentially enhance stability by modifying interfacial charge transport and improving the interaction between the sensing surface and target gas molecules. The long-term stability of ZnO, SnO_2, and ZnO-SnO_2 sensors was evaluated over a period of 20 days as shown in Fig.9. The ZnO-SnO_2 composite presented a nearly constant response, while SnO_2 and ZnO maintained relatively slight difference. The negligible fluctuations indicate excellent response stability and reproducibility, highlighting the potential of the composite for reliable gas-sensing applications under ambient conditions.

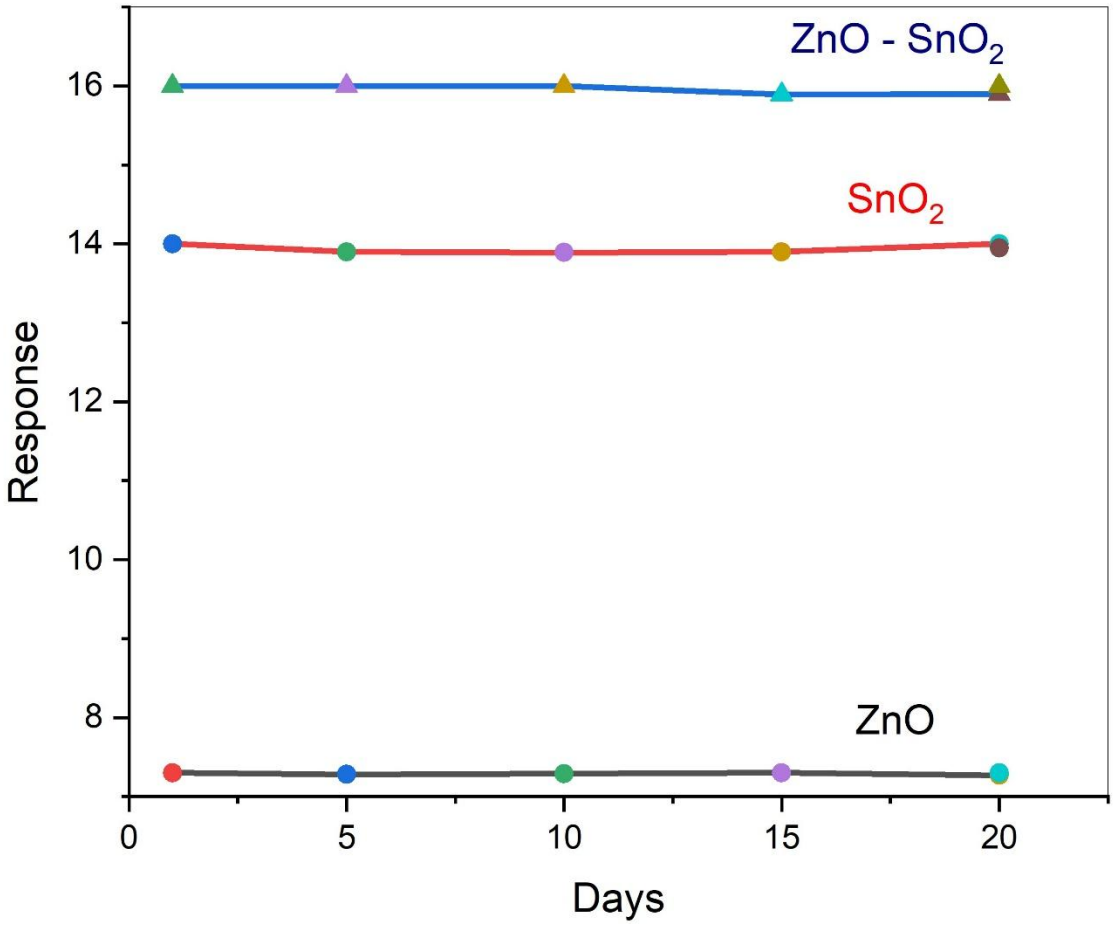


Fig.9. Long term stability of various gas sensors towards 5 ppm of formaldehyde

4.3. Transient response characteristics

The transient response-recovery characteristics of the ZnO, SnO_2 and ZnO-SnO_2 sensors were evaluated by monitoring resistance variations during 5 ppm of formaldehyde gas exposure and subsequent recovery in air. The response time is defined as the time required for the sensor to achieve 90% of its total resistance change after introducing the target gas, whereas the recovery time is the time required to restore 90% of the original resistance change after removing the gas [42]. As shown in the figure, the sensor resistance decreases during gas exposure, indicating effective interaction between the reducing gas molecules and adsorbed oxygen species. The subsequent increase in resistance results from oxygen re adsorption onto the sensing surface. These reversible resistance changes demonstrate effective gas detection and recovery behaviour, highlighting the potential of the sensing material for practical gas-sensing applications. From the fig.10, response/recovery times towards ZnO, SnO_2 and ZnO-SnO_2 determined as 65s/60s, 52s/35s and 36 s/24 s respectively.

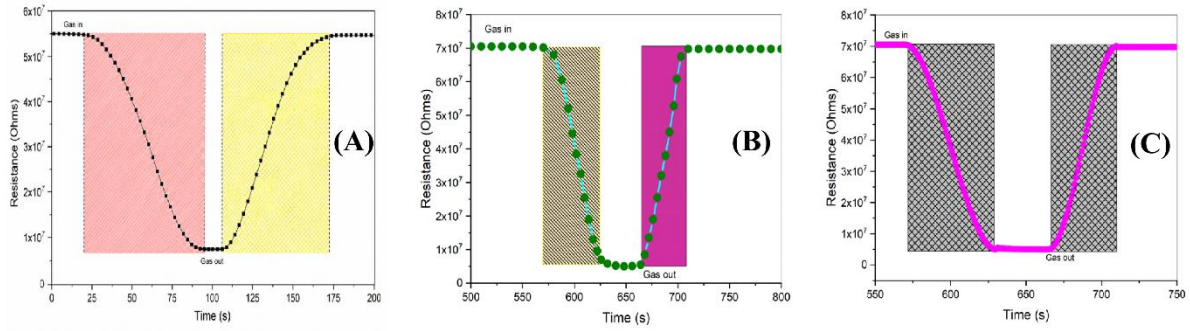


Fig.10 Transient response characteristics of (A) ZnO, (B) SnO_2 and (C) ZnO-SnO_2 composites towards 5 ppm of formaldehyde at room temperature

Table 2 presents a comparative evaluation of the formaldehyde-sensing performance of the prepared ZnO, SnO_2, and ZnO-SnO_2 composite sensors against recent reported metal oxide-based sensors. Among the investigated materials, the ZnO-SnO_2 composite exhibits the highest response of 16 towards 5 ppm formaldehyde under ambient conditions, exceeding those of pristine ZnO (7.3) and SnO_2 (14). Furthermore, the composite demonstrates quick response and recovery times of 36 and 24 s, respectively, showing improved sensing kinetics. Although several recent reported sensors demonstrate high responses, working at elevated temperatures, which can increase power utilisation and complicate practical deployment. The enhanced performance of the present composite may be associated with the synergistic interaction between ZnO and SnO_2, the decreased crystallite size, and the formation of n-n heterointerfaces that facilitate charge-carrier modulation during formaldehyde exposure.

Table.2. Comparative table of various metal oxide gas sensors toward formaldehyde

S. No	Material	Concentration (ppm)	Operating Temperature (ºC)	Response	Res/Rec time (s)	Ref
1	ZnO	100	220	9.5	1/12	[43]
2	Al doped ZnO	20	350	95.5	-	[44]
3	ZnO@ZIF-8	5	Room temperature	2.1	68/150	[45]
4	Zn doped SnO_2	10	400	25.7	12/45	[46]
5	Y doped SnO_2	50	180	18	8/10	[47]
6	Li doped ZnO	100	350	40.2	8/26	[48]
7	SnO_2	100	200	38.3	17/25	[49]
8	Sb doped SnO_2	5	Room temperature	4.9	98/74	[50]

9	SnO_2-ZnO	20	200	9.7	27/89	[51]
10	ZnO-SnO_2	1	300	56	110/245	[52]
11	ZnO	100	Room temperature	1.88	97/86	[53]
12	Cd doped SnO_2	100	160	51.11	28/104	[54]
13	ZnO	5	Room temperature	7.3	65/60	Present study
14	SnO_2	5	Room temperature	14	52/35	
15	ZnO-SnO_2	5	Room temperature	16	36/24	

Conclusions

In the present study, pure ZnO, SnO_2, and ZnO-SnO_2 nanocomposites were successfully synthesized using a facile hydrothermal technique and systematically investigated for room-temperature formaldehyde detection. The structural and morphological investigations confirmed the coexistence of hexagonal wurtzite ZnO and tetragonal rutile SnO_2 phases in the composite. X-ray diffraction studies revealed a reduction in the average crystallite size from 9.60 nm for ZnO and 7.30 nm for SnO_2 to 5.97 nm for the ZnO-SnO_2 composite, indicating suppressed crystallite growth and the formation of additional interfacial regions. SEM and TEM studies further demonstrated the integration of ZnO crystallites with fine SnO_2 nanoparticles, providing a heterogeneous morphology favourable for gas adsorption and charge transport. Raman spectroscopy and XPS measurements supported the presence of the constituent metal oxide phases and their corresponding chemical oxidation states. Gas-sensing investigations demonstrated that the ZnO-SnO_2 composite exhibited the highest response towards 5 ppm of formaldehyde at room temperature, achieving a response value of 16, compared with 7.3 for ZnO and 14 for SnO_2. The composite also shown shorter response and recovery times of 36 and 24 s, respectively, outperforming the individual oxide sensors. Selectivity measurements presented a stronger response towards formaldehyde than other interfering vapours such as acetone, methanol, ethanol, and benzene. Furthermore, the composite maintained a nearly constant response during a period of 20-day stability evaluation. These improvements are attributed to the combined synergetic effects of nanoscale crystallites, accessible surface sites, and interfacial charge modulation associated with the n-n heterostructure.

Author contributions:

The manuscript was written through the contributions of both the authors. Both the authors have approved the final version of the manuscript.

Funding

The authors did not receive any funding from any organization for the submitted work.

Data availability:

The datasets used and/or analyzed during the current study are available from the corresponding author on reasonable request.

Declarations Conflict of interest :

The authors declare no competing interests.

References

[1] Yuting Shuai, Wanteng Peng, Qiangyong Tang, Wenhao Shen, High-performance formaldehyde gas sensor based on flower-like $ZnCo_2O_4/In_2O_3$ heterostructures, Sensors and Actuators B: Chemical, 442, 2025, 138112.

[2] L. Zhu, J. Wang, J. Liu, Z. Xu, M.S. Nasir, X. Chen, Z. Wang, S. Sun, Q. Ma, Z. Wang, J. Feng, L. Ji, W. Yan, In situ enrichment amplification strategy enabling highly sensitive formaldehyde gas sensor, Sensors and Actuators B: Chemical 354 (2022) 131206.

[3] K. GangaReddy, P. Nagaraju, G.L.N. Reddy, P. Ghosal, M.V. Ramana Reddy, Growth and characterization of electron beam evaporated NiO thin films for room temperature formaldehyde sensing, Sensors and Actuators A: Physical 346 (2022) 113876.

[4] P.C. Yao, P.Y. Chu, D.H. Shih, W.C. Liu, Formaldehyde gas sensing properties of a sputtered indium tin zinc oxide thin film decorated with evaporated gold nanoparticles, Sensors and Actuators B: Chemical 412 (2024) 135824.

[5]] J.G. Kang, J.S. Park, H.J. Lee, Pt-doped SnO_2 thin film based micro gas sensors with high selectivity to toluene and HCHO, Sens. Actuators B Chem. 248 (2017) 1011–1016.

[6] A. Sharma, S.B. Eadi, H. Noothalapati, M. Otyepka, H.-D. Lee, K. Jayaramulu, Porous materials as effective chemiresistive gas sensors, Chemical Society Reviews 53 (2024) 2530–2577.

[7] S.G. Dasari, P. Nagaraju, V. Yelsani, M.V. Ramana Reddy, Mesoporous sieve structured ITO-based thin films for enhanced formaldehyde detection, Journal of Materials Science: Materials in Electronics 33 (30) (2022) 23447–23467.

[8] Turlybekuly, A., Shynybekov, Y., Soltabayev, B., Yergaliuly, G., Mentbayeva, A., The Cross-Sensitivity of Chemiresistive Gas Sensors: Nature, Methods, and Peculiarities: A Systematic Review, ACS Sensors 9 (12) (2024) 6358–6371.

[9] Krishna, K. G., Parne, S., Pothukanuri, N., Kathirvelu, V., Gandi, S., Joshi, D. Nanostructured metal oxide semiconductor-based gas sensors: A comprehensive review. Sensors and Actuators A: Physical, 341, (2022),113578.

[10] P.K. Panigrahi, B. Chandu, N. Puvvada, Recent Advances in Nanostructured Materials for Application as Gas Sensors, ACS Omega 9 (3) (2024) 3092–3122.

[11] P. Nagaraju, Y. Vijayakumar, G.L.N. Reddy, M.V. Ramana Reddy, ZnO wrinkled nanostructures: Enhanced BTX sensing, Journal of Materials Science: Materials in Electronics 29 (2018) 11457–11465.

[12] Shaikh T, Jain S. ZnO nanostructure-based gas sensors: Critical review based on their synthesis and morphology towards various oxidizing and reducing gases. Current Nanomaterials. 2023;8(4):336–360.

[13] Zhang X, Sun J, Tang K, Wang H, Chen T, Jiang K, Zhou T, Quan H, Guo R. Ultralow detection limit and ultrafast response/recovery of the H_2 gas sensor based on Pd-doped rGO/ZnO-SnO_2 from hydrothermal synthesis. Microsystems & Nanoengineering. 2022;8:67.

[14] Liu Z-L, Yang Z, Liu B, Chen Y-N, Feng W. Construction of Hybrid ZnO/SnO_2 n–n heterojunction with hierarchical porous biomorphic nanostructure as a high-response sensor for methanol gas. Crystals. 2024;14(12):1049.

[15] Xue L, Li Y, Deng Y. Multicomponent porous metal oxide semiconductors for advanced gas sensing. Micro & Nano Science. 2025; 1:2.

[16] Panigrahi, P. K.; Chandu, B.; Puvvada, N. Recent Advances in Nanostructured Materials for Application as Gas Sensors. ACS Omega, 9 (2024) 3092–3122.

[17] Gupta, V. K.; Alharbie, N. S.; Agarwal, S.; Grachev, V. A. New Emerging One-Dimensional Nanostructure Materials for Gas Sensing Application: A Mini Review. Current Nanoscience, 15 (2019) 131–135.

[18] Jung D. N-type metal oxide semiconductor hydrogen sensors: mechanisms, materials design, and interface engineering strategies, Nanomaterials, 2026;16(12):762.

[19] Du, L.; Sun, H. Facile synthesis of ZnO/SnO_2 hybrids for highly selective and sensitive detection of formaldehyde. New Journal of Chemistry 2022, 46, 4753–4761.

[20] Park, J.; Chaulagain, D.; Ngando Same, N.; Yakub, A. O.; Lim, J. O.; Roh, J. W.; Huh, J. S., Formaldehyde gas response and selectivity of ZnO-SnO_2 gas sensors. Sensors and Actuators B: Chemical 2025, 425, 136958.

[21] He, C.S.; Ye, J.C.; Zhang, H.H.; Gong, X.; Li, X. A review: Strategies for enhancing the performance of SnO_2-based formaldehyde gas sensors. Microchemical Journal 2025, 208, 112591.

[22] V. Suresh, Pothukanuri Nagaraju , Velavan Kathirvelu, Saidi Reddy Parne, Jack Julies Joe Jeyaselan, Synthesis and characterization of ZnO and ZnO-MoO_3 composite thin films ethanol detection, Next Materials 13 (2026) 102961.

[23] Sandeep Kumar, Deepika Kaushal, Biogenic synthesis of ZnO nanoparticles using Woodfordia fruticosa extract for enhanced antibacterial and photocatalytic performance, Next Materials, 13, (2026), 102629.

[24] K. Ravichandran, K. Gayathri, M. Baneto, B. Kaleeswaran, P.K. Praseetha, B. Deepa, N. Anuradha, Photocatalytic dye detoxification by cost-effective SnO_2:Ce thin films and verification of toxicity by histology using Labeo rohita fish, Process Biochemistry, Volume 156, (2025), 118-135.

[25] Nor Diyana Md Sin, Mohamad Hafiz Mamat, Mohamad Zhafran Hussin, Dayana Kamaruzaman, M. Rusop, Enhancement of ZnO/SnO_2 composite-based humidity sensors through porous growth at different oxygen ratios, Materials Today Communications, 50, (2026), 114322.

[26] Xingkun Liang, Rong Dai, Hao Ma, Xiaoning Tang, Bin Zhang, Synergistic antibacterial properties of ZnO-SnO_2 composite under both light and dark conditions, Ceramics International, 48, (2022), 32089-32103.

[27] Vineeta Yadav, Nirmal Singh, Deshraj Meena, Investigation of structural and optical properties of pure SnO_2, ZnO and SnO_2/ZnO composite nanorods, Materials Today: Proceedings, 62, (2022), 3368-3375.

[28] Mayur Lagariya, Mansi Modi, Himanshu Dadhich, Manan Gal, Keval Gadani, P.S. Solanki, N.A. Shah, Studies on structural and electrical behaviours of chemically grown ZnO/SnO_2 nanocomposites, Physica B: Condensed Matter, 577, (2020), 411774.

[29] Srinivasa Rao Sriram, Saidi Reddy Parne, Nagaraju Pothukanuri, Dhananjay Joshi, Damodar Reddy Edla; Facile Synthesis of Pure and Cr-Doped WO_3 Thin Films for the Detection of Xylene at Room Temperature. ACS Omega 27 December 2022; 7 (51): 47796–47805.

[30] Astriyani MN, Suyatma NE, Armetha V, Purnomo EH, Muhandri T, Budi FS, Abbes B, Tara A. Top-Down ultrasonication method for ZnO nanoparticles fabrication and their application in developing pectin-glycerol bio nanocomposite films. Physchem. 2025;5(4):42.

[31] Vallimeena S, Helina B. Cauliflower-like strontium-doped SnO_2 nanoparticles for photocatalytic degradation. Materials Science and Technology. 2023;39(16):2277–2286.

[32] M. Abd Mutalib, M.A. Rahman, M.H.D. Othman, A.F. Ismail, J. Jaafar, Chapter 9 - Scanning Electron Microscopy (SEM) and Energy-Dispersive X-Ray (EDX) Spectroscopy, Editor(s): Nidal Hilal, Ahmad Fauzi Ismail, Takeshi Matsuura, Darren Oatley-Radcliffe, Membrane Characterization, Elsevier, 2017, Pages 161-179, ISBN 9780444637765.

[33] Ashraful Bari Anik, Mofassel Hossen Akash, Md. Ashraful Alam, Md. Zahangir Alam, Debanjon Sarker, Nahid Sultana, Green synthesis of ZnO nanoparticles using Justicia adhatoda for effective photocatalytic degradation of methylene blue dye, RSC Advances, Volume 15, Issue 54, 2025, Pages 45874-45888, ISSN 2046-2069.

[34] Muchuweni, E., Sathiaraj, T. S., & Nyakotyo, H. Synthesis and characterization of zinc oxide thin films for optoelectronic applications. Heliyon, 3(4), (2017), e00285.

[35] Sangeetha, P., Sasirekha, V., & Ramakrishnan, V. Micro-Raman investigation of tin dioxide nanostructured material based on annealing effect. Journal of Raman Spectroscopy, 42(8), (2011)1634-1639.

[36] Almoneef, M. M., Awad, M. A., Aldosari, H. H., Hendi, A. A., Aldehish, H. A., Merghani, N., & Alshammari, S. G., Exploring the multi-faceted potential: Synthesized ZnO nanostructure - Characterization, photocatalysis, and crucial biomedical applications. Heliyon, 10, (2024), e32714.

[37] Sweety, M. N., Sultana, S., Alam, M. A., Chowdhury, F., Tasnim, A., Islam, S., Shathi, A. S. Green synthesis of wurtzite ZnO nanoparticles via Indigofera tinctoria stem extract: linking crystallinity with photocatalytic and biological performance. Nanoscale Advances, 8(19), (2026), 5567–5586.

[38] Qin, S., Tang, P., Feng, Y., Li, D., Novel ultrathin mesoporous ZnO-SnO_2 n-n heterojunction nanosheets with high sensitivity to ethanol. Sensors and Actuators B: Chemical, 309,(2020) 127801

[39] Gurylev, V., Perng, T.P., Defect engineering of ZnO: Review on oxygen and zinc vacancies, Journal of the European Ceramic Society 41, (2021), 4977–4996.

[40] Y. Hu, L.J. Cao, Y.P. Gong, X. Ma, Y.F. Chen, T. Jin Novel SnO2/ZnO gas-sensitive materials for high formaldehyde selectivity constructed by way of doping Sn into ZIF-8 J. Alloy. Compd., 1036 (2025), 18201.

[41] Dasari, S. G., Nagaraju, P., Yelsani, V., Ramana Reddy, M. V., Mesoporous sieve structured ITO-based thin films for enhanced formaldehyde detection, Journal of Materials Science: Materials in Electronics, 33(2022), 23447-23467.

[42] Nagaraju, P., Vijayakumar, Y., Ramana Reddy, M. V., Effect of oxygen partial pressure on the microstructural, optical and gas sensing characterization of nanostructured Gd doped ceria thin films deposited by pulsed laser deposition. Journal of Asian Ceramic Societies, 5, (2017) 402-409.

[43] Wang, S., Cao, J., Cui, W., Fan, L., Li, X., Li, D., Constructing chinky zinc oxide hierarchical hexahedrons for highly sensitive formaldehyde gas detection. Journal of Alloys and Compounds, 775, (2019) 402-410.

[44] Chi, C.-Y., Chen, H.I., Chen, W.C., Chang, C.H., Liu, W.C., Formaldehyde sensing characteristics of an aluminum-doped zinc oxide (AZO) thin-film-based sensor. Sensors and Actuators B: Chemical, 255, (2018) 3017–3024.

[45] Reddy, A. J. M., Katari, N. K., Nagaraju, P., Reddy, K. H., & Surendra Babu, M. S. (2021). Fabrication and deployment of nanodisc ZnO@ZIF-8, ZnO@NA and ZnO@INA core–shell MOFs: enhanced NH_3 and HCHO gas sensing. Journal of Materials Science: Materials in Electron.

[46] Zhu, L., Wang, J., Liu, J., Nasir, M. S., Zhu, J., Li, S., Liang, J.,Yan, W., Smart formaldehyde detection enabled by metal organic framework-derived doped electrospun hollow nanofibers. Sensors and Actuators B: Chemical, 326, 128819.nics, 32(6),(2021) 7827–7840.

[47] K. Zhu, S. Ma, Y. Tie, Q. Zhang, W. Wang, S. Pei, Highly sensitive formaldehyde gas sensors based on Y-doped SnO_2 hierarchical flower-shaped nanostructures, J. Alloy. Compd. 792 (2019) 938–944.

[48] Zhao JW, Xie CS, Yang L, Zhang SP, Zhang GZ, Cai ZM. Enhanced gas sensing performance of Li-doped ZnO nanoparticle film by the synergistic effect of oxygen interstitials and oxygen vacancies. Appl Surf Sci. 330, (2015) 126-33.

[49] Chengming Lou, Chen Yang, Wei Zheng, Xianghong Liu, Jun Zhang, Atomic layer deposition of ZnO on SnO2 nanospheres for enhanced formaldehyde detection, Sensors and Actuators B: Chemical, Volume 329, 2021, 129218.

[50] Thirukachhi Suvarna, K. Ganga Reddy, Varishetty Madhu Mohan, Gunja Lavanya, M.V. Ramana Reddy, C.P. Vardhani, Investigation on Sb-doped SnO2 as an efficient sensor for the detection of formaldehyde, Materials Today Communications, 37, (2023), 107438

[51] C. Lou, C. Yang, W. Zheng, X. Liu, J. Zhang, Atomic layer deposition of ZnO on SnO_2 nanospheres for enhanced formaldehyde detection, Sens. Actuators B: Chem. 329 (2021) 129218.

[52] Park J, Chaulagain D, Same NN, Yakub AO, Lim JO, Roh JW, Huh JS. Formaldehyde gas response and selectivity of ZnOSnO2 gas sensors. Sens Actuators B Chem. 2025;425:136958.

[53] Guo W., Zhao B., Huang L., He Y. One-step synthesis of ZnWO4/ZnSnO3 composite and the enhanced gas sensing performance to formaldehyde Mater. Lett., 277 (2020), 128327.

[54] R. Zhao, X. Zhang, S. Peng, P. Hong, T. Zou, Z. Wang, X. Xing, Y. Yang, Y. Wang Shaddock peels as bio-templates synthesis of Cd-doped SnO2 nanofibers: A high performance formaldehyde sensing material J. Alloys Compd., 813 (2020), 152170.